Journal of Materials Research and Technology 38 (2025) 2010–2015

Contents lists available at ScienceDirect

Journal of Materials Research and Technology

journal homepage: www.elsevier.com/locate/jmrt

Ultrasonic study of polycrystalline TMZF alloy at cryogenic temperatures

Ariel Omar Moreno Gobbi [a], Paulo Sergio Silva Junior [b], Diego Rafael Nespeque Correa [c], Rafael Formenton Macedo dos Santos [d,e], Javier Andrés Muñoz Chaves [f], Carlos Roberto Grandini [c], Conrado Ramos Moreira Afonso [d,e,*]

[a] UdelaR, Institute of Physics, Faculty of Sciences, Ultrasonic Acoustics Laboratory, Igua, Montevideo, 4225, Uruguay
[b] Universidade Federal de São Carlos (UFSCar), Department of Physics, São Carlos, 13565-905, SP, Brazil
[c] São Paulo State University (UNESP), School of Sciences, Laboratorio de Anelasticidade e Biomateriais, Bauru, 17.033-360, SP, Brazil
[d] Universidade Federal de São Carlos (UFSCar), Graduate Program in Materials Science and Engineering (PPG-CEM), São Carlos, 13565-905, SP, Brazil
[e] Universidade Federal de São Carlos (UFSCar), Department of Materials Engineering (DEMa/BioMet-CAM), São Carlos, 13565-905, SP, Brazil
[f] Corporación Universitaria Comfacauca-Unicomfacauca, Faculty of Engineering, Intelligent System Research Group, Popayan, 190003, Colombia

ARTICLE INFO

Keywords:
Ti alloy
TMZF
Cryogenic temperature
Phase transition
Ultrasonic characterization

ABSTRACT

In this study, the phase stability of the polycrystalline TMFZ (Ti–12Mo–6Zr–2Fe, wt%) alloy, produced by electron beam melting and thermomechanically processed through swaging, was evaluated by ultrasonic measurements at cryogenic temperatures. XRD and SEM analyses at room temperature confirmed the presence of a major β phase as equiaxial grains and a minor α" phase in the form of acicular structures. Ultrasonic measurements were realized with 10 MHz ultrasonic pulses and the pulse-echo technique in cooling-heating cycles of temperature between room temperature and 150 K. Some anomalies in the ultrasonic attenuation and velocity at cryogenic temperatures were related to the alloy's phase transitions in the temperature range investigated. The anomaly observed at the lowest temperature investigated was compared with the diagram calculated using the CALPHAD, which predicted the formation of an ω phase (bcc crystalline structure) at low temperatures. This finding also supported some theoretical phase predictions for Ti's solid solutions. Detection of the α → ω phase transition at cryogenic temperatures in the TMFZ alloy can open new horizons for novel industrial applications, particularly those operating under extreme temperature conditions.

1. Introduction

Current research has demonstrated the promising potential of β-type Ti alloys (with a bcc crystal structure) in various applications, including medical, aerospace, aeronautics, automotive, and marine sectors. In particular, the TMZF alloy (Ti–12Mo–6Zr–2Fe, wt%) is one of the most notable commercial β-type Ti alloys, due to its exceptional combination of higher specific strength, lower elastic modulus, improved corrosion resistance, and recognized biocompatibility [1,2]. The manufacturing process of β-type Ti alloys involves alloying with sufficient β-stabilizer elements to prevent the formation of α phase (hcp crystal structure) after quenching [3,4]. Thus, the final phase composition of the β metastable solid solution can comprise the metastable α', α", and ω phases, which depend on the chemical composition and play a crucial role in its properties [5–7]. The relationship between the phase composition and mechanical properties of β-type Ti alloys is relevant to industrial applications, as it has been found that the martensitic α" phase is responsible for producing superelasticity and shape memory effects. In contrast, the ω phase is detrimental to the increasing hardness and elastic modulus [8–10]. Furthermore, the elastic modulus tends to decay in proportion to the amount of β phase, hindering the stress-shielding effect in biomedical Ti-based alloys [11,12].

The phenomena of phase transition in Ti alloys can be experimentally investigated by a variety of characterization techniques, including electrical resistance measurements [13], differential scanning calorimetry (DSC), differential thermal analysis (DTA) [14,15], and mechanical relaxation analysis [16]. The last one can provide a deep insight into the micro- and nano-scale defects that affect the mechanical performance at the macro-scale, and also enable the study of dynamic processes because is a sensitive physical property involving mechanical energy absorption by the structural arrangement, phase transition, diffusion, and matrix-solute interaction (interstitial and/or substitutional), among

* Corresponding author. Universidade Federal de São Carlos (UFSCar), Graduate Program in Materials Science and Engineering (PPG-CEM), São Carlos, 13565-905, SP, Brazil

https://doi.org/10.1016/j.jmrt.2025.08.035
Received 3 June 2025; Received in revised form 25 July 2025; Accepted 5 August 2025
Available online 7 August 2025

other mechanisms [17]. For example, using frequencies of 5 and 10 MHz, Moreno-Gobbi et al. [18] recently investigated low-temperature transformations in a Ni–Ti alloy using an ultrasonic pulse-echo technique combined with XRD, TEM, and DSC, revealing a series of phase changes and structural rearrangements. Therefore, the ultrasonic technique has been established as a powerful tool for accurately detecting and characterizing phase transitions in Ti alloys at temperatures below room temperature (RT).

In recent years, advances in computing have enabled the integration of experimental results with numerical simulation techniques, facilitating the interpretation of anomalies observed in experimental data. In this scenario, the CALPHAD method has been frequently used to predict the phase composition and properties of materials by calculating phase equilibria and transformations using thermodynamic models. In Ti-based alloys, it has been valuable to optimize the chemical composition to achieve the desired properties with reduced experimental effort. For example, the CALPHAD method has been successfully applied in the design of low-cost and high-strength Ti–Al–Cr and Ti–Al–Fe alloys, or even high entropy alloys, for engineering applications [19–21].

In line with the current interest in β-type Ti alloys for industrial applications and the ability to detect atomic rearrangements and phase transformations by ultrasonic measurements, this study aimed to evaluate the ultrasonic velocity and attenuation of the TMFZ alloy (Ti–12Mo–6Zr–2Fe, wt%) at cryogenic temperatures. Additionally, DSC measurements and theoretical calculations of the phase composition were performed to support the interpretation of the ultrasonic results.

2. Materials and methods

The Ti–12Mo–6Zr–2Fe (TMZF, wt.%) alloy was produced from commercially pure raw metals using the Electron Beam Melting (EBM) technique in a water-cooled copper mold under an inert argon atmosphere. Then, the ingot underwent rotary-forging (swaging) thermomechanical treatment at 1173 K until it reached a cross-sectional diameter of ~10 mm (resulting in an area reduction of around 79 %), followed by air cooling (named here as TMZF sample). Further processing details can be found in earlier studies from our group [22–24].

The phase composition was evaluated using X-ray diffraction (XRD) with a Rigaku Gierflex model, operating at 40 kV and 25 mA in the θ-2θ configuration, with a scan speed of 0.02°/s. The XRD pattern was later evaluated using crystallographic data sheets from the COD (Crystallographic Open Database). Differential scanning calorimetry (DSC; Netzsch 200 F3 Maia equipment) was used to investigate phase transitions below room temperature. The DSC test was conducted in the temperature range from 298 K to approximately 123 K at a cooling rate of 10 K/min. The DSC results were compared with the predicted phase diagram acquired by ThermoCalc® software (SGTE PURE5 database). Microstructural details were evaluated by optical microscopy (OM; Olympus BX41M-LED) and scanning electron microscopy (SEM; Philips FEG XL30F) coupled with an X-ray energy dispersive spectroscopy (EDS; EDAX detector) device. For this purpose, the sample was subjected to standard metallographic preparation, which involved abrasion with SiC emery papers (from #240 to #1500 mesh), polishing with alumina (1 μm), and etching in a modified Kroll's solution (40 % H_2O, 40 % HF, and 20 % HNO_3). Preliminary mechanical properties were evaluated by measuring elastic modulus and Vickers microhardness at room temperature. The impulse excitation method was employed to determine the elastic modulus using the Sonelastic equipment (ACTP Physical Engineering Inc., Brazil). Vickers microhardness was measured in a Shimadzu microhardness model HMV-G 20 ST.

The conventional pulse-echo ultrasonic technique was employed for ultrasonic measurements, utilizing X-cut quartz transducers with a 10 MHz fundamental frequency. Attenuation and pulse travel time were measured simultaneously in cooling-warming temperature cycles [25]. A sample was cut from the original ingot for these measurements, in the form of a cylinder (Ø10 mm × 12 mm). Then, the two plane faces were

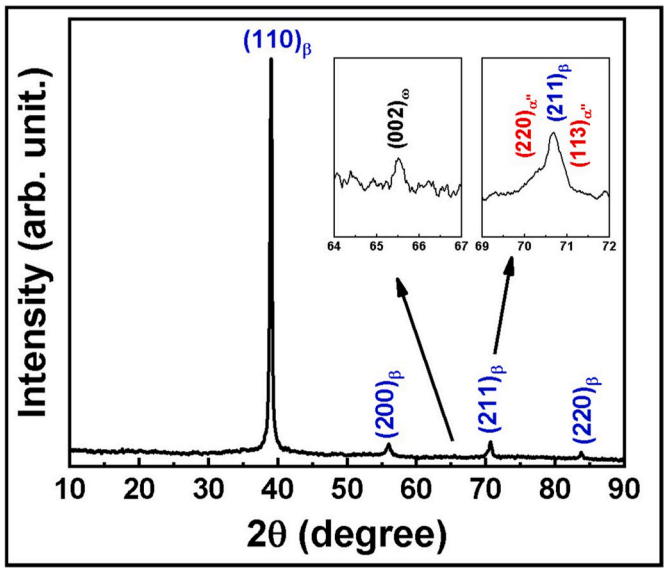

Fig. 1. XRD profile of the as-received TMZF alloy sample.

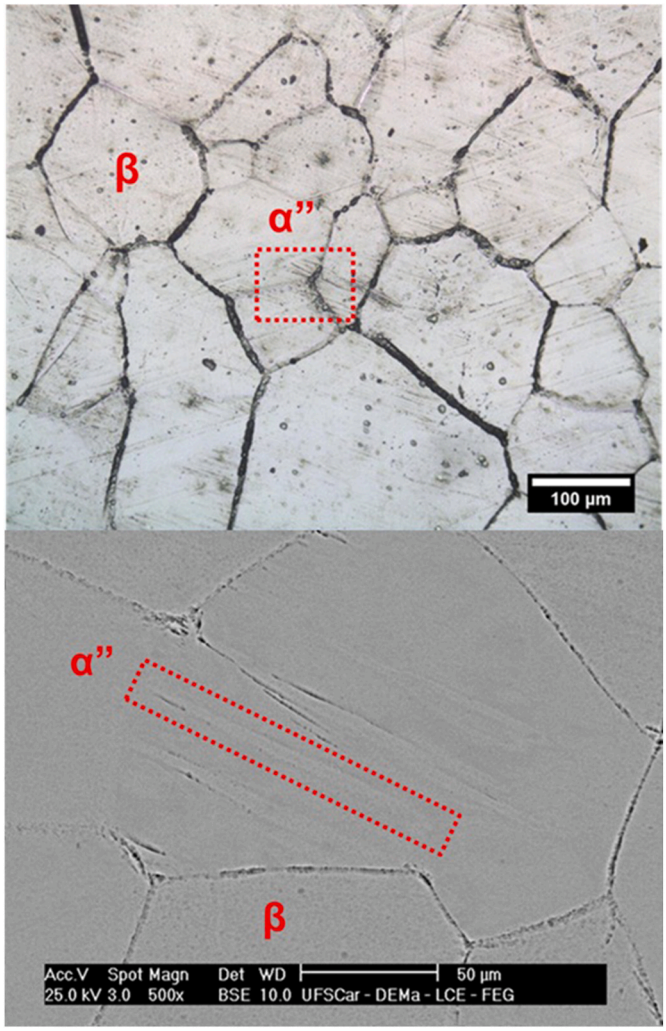

Fig. 2. Optical microscopy (top) and SEM imaging in BSE mode (bottom) of the as-received TMZF sample.

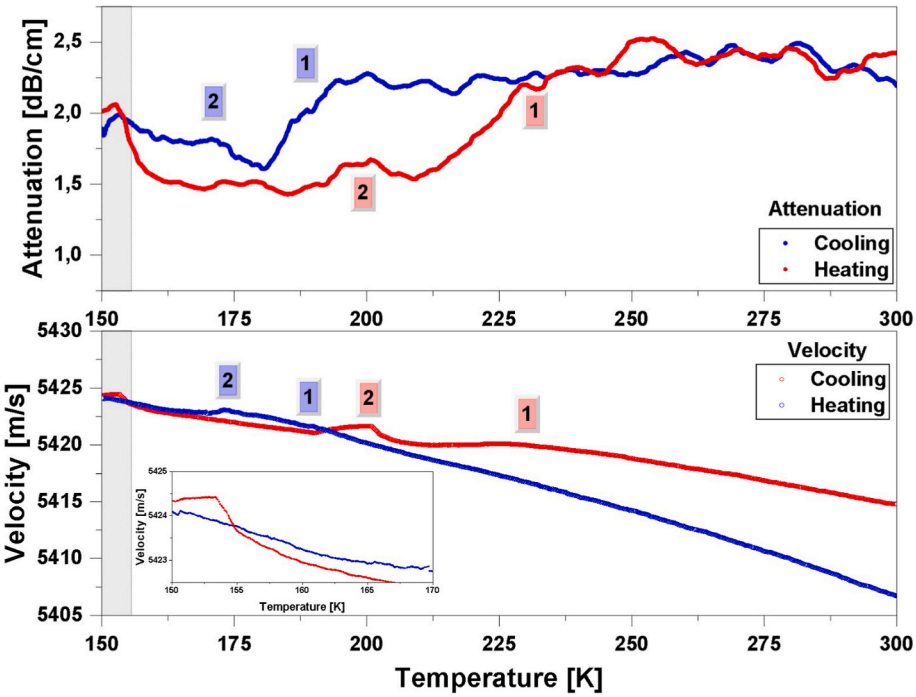

Fig. 3. Ultrasonic attenuation and sample velocity TMZF, showing cooling (blue) and heating (red) processes. The numbers label different anomalies on the curves. The inset shows the process in the shaded region in detail.

mechanically polished for ultrasonic measurements as described in previous work [26]. The ultrasonic transducer was bonded to the sample face with a Nonac Stopcock Grease. An ultrasonic pulse generator was used in conjunction with a liquid nitrogen cryostat, and the experimental setup was fully automated for measuring and monitoring temperature, as well as heating and cooling rates. Measurements were performed during cooling from room temperature (RT) to 130 K at a constant rate of 1 K/min to avoid thermal gradients in the sample and maintain it near thermal equilibrium. As described in a previous paper [18], the absolute round-trip transit time for the ultrasonic wave was initially determined between two consecutive echoes. Then, the transit round-trip time variations were accurately measured using cross-correlation techniques over a selected echo. Ultrasonic attenuation was obtained by monitoring two echoes in video mode, comparing the areas between two selected echoes.

3. Results and discussion

3.1. Phase composition, microstructure, and mechanical aspects at room temperature

The phase composition and microstructure of the as-received sample are depicted in Figs. 1 and 2. The XRD profile (Fig. 1) exhibited intense peaks from the β phase and faint peaks from the ω and martensitic α" phase, following some previous studies in the literature with similar metastable β-type Ti alloys [27,28]. The microstructure (Fig. 2) was composed of equiaxed β phase grains in the order of dozens of micrometers and some thin acicular structures, with smooth Z-contrast in the BSE image, related to α" phase. The sample also exhibited a Vickers micro-hardness value of approximately 338 HV and an elastic modulus of around 80 GPa at room temperature, which differed from those of commercially pure Ti grade 2 (~180 HV and 100 GPa) with a single α phase, and agreed well with previous studies in the literature [29]. Considering the elevated amount of β-stabilizer alloying elements in solid solution and the thermomechanical processing of the sample, the dual-phase composition, having a major β phase with traces of the metastable α" phase, is typical for metastable β-Ti alloys, suggesting a phase transition of β → α" upon quenching. In this sense, the obtained micro-hardness values and elastic modulus for the TMZF alloy can be linked with the chemical and phase composition aspects of the solid solution [30].

The obtained phase composition is also aligned with the theoretical predictions for the design of Ti alloys. According to the Al-Mo_{eq} concept [31], the TMZF alloy possesses a Mo_{eq} value between 18 and 19, corresponding to a metastable β-type Ti alloy with the M_s line for the martensitic α" phase close to the room temperature and within the region for metastable ω phase formation [32]. From the Bo-Md diagram's point of view [30], the TMZF alloy has a Bo value equal to 2.816 and a Md value of 2.404, placing it in the β phase field, and is quite close to the M_s line for the martensitic α" phase and β + ω line as well. Furthermore, the TMZF alloy exhibited an electron-to-atom ratio of 4.20, located at the interface between the α" + β and β + ω phases [33]. According to the ASTM F1813-01 standard [34], the TMZF alloy can only remain in a full β phase on the microstructure after rapid cooling from temperatures above 998 K. Therefore, considering the thermomechanical history of the sample, the occurrence of β → ω phase transition in the sample is probable, resulting in a β + α" + ω phase composition in the sample at room temperature. Lastly, the obtained result agreed well with the phase composition detected by Guerra et al. [35] and Nag et al. [36], who identified ω phase formation on the β phase matrix of the TMZF alloy induced by hot deformation or ageing treatment.

3.2. Ultrasonic and thermal evaluation at cryogenic temperatures

Fig. 3 shows the ultrasonic attenuation and velocity measured on the TMZF sample during a cooling-heating cycle between room temperature and 150 K. A quartz transducer with an X-cut orientation and a central frequency of 10 MHz was used for our measurements. To avoid temperature gradients in the sample, the sample temperature varied at a rate of 2 K/min. The attenuation-velocity spectrum at temperatures below room temperature, as shown in Fig. 3, provides information on the internal mechanisms of the sample, including an unexpected equilibrium phase transformation detected at approximately 160 K, which will be discussed later. Although the attenuation-velocity spectrum shows a

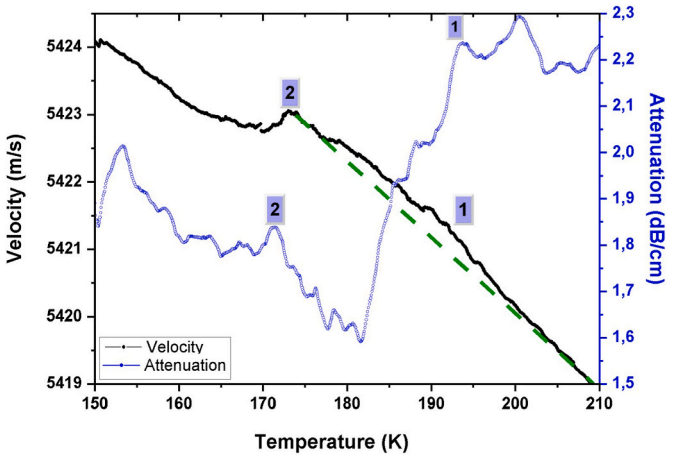

Fig. 4. Ultrasonic attenuation and velocity in the cooling run for TMZF alloy, amplified in the reduced temperature interval between 150 K and 210 K.

complex behaviour, at least three main anomalies can be observed in both branches of the temperature cycle.

During the cooling run, at least three evident anomalies in the attenuation can be observed at approximately 200 K, 175 K, and 160 K, respectively, accompanied by corresponding changes in the velocity. Near 200 K, an abrupt decrease in attenuation is observed, extending up to 180 K. At 175 K and 160 K, two distinct peaks are present. On the other hand, in the heating run, a distinct peak is observed in the attenuation at 160 K and 200 K, accompanied by an abrupt increase from 220 K up to 230 K. Velocity profile analysis reveals a distinct anomaly at 175 K during the cooling cycle and a comparable discontinuity at 200 K during the heating cycle, with the observed correspondence between the attenuation peaks at these temperatures suggesting that the phenomenon may arise from the same underlying mechanism. Additionally, a similar behaviour is observed in velocity up to the beginning of the anomaly in attenuation at 200 K in the cooling run and 220 K in the heating run, indicating a correspondence between the observed attenuation steps. These anomalies, which can be observed in both attenuation and speed simultaneously, are labelled as 1 and 2 to distinguish them from other minor alterations that can be attributed to the complex behaviour of the deformed sample. The anomalies tagged as number 3 are not hysteretic, and we attribute them to a possible and unexpected low-temperature phase transition.

We attributed the anomaly labelled as 1, which exhibits a large temperature hysteresis, to a martensitic phase transition, as expected for the studied TMZF sample based on the crystalline phases observed during structural characterization performed at room temperature. Finally, the anomaly tagged as 2 is identified as a secondary peak accompanying the previously mentioned main martensitic transformation. Details of the attenuation and velocity variations are presented in Fig. 4, where an abrupt decrease in velocity is observed at the same temperature as the attenuation peak. This secondary peak is similar to the one observed by us in the ultrasonic characterization of a Ni–Ti alloy at low temperatures, where this anomaly was correlated with a marked shift in the morphology of martensite domain interfaces, encompassing both phase and twin interfaces, during the progression of martensite phase formation. This morphological shift induced a temperature decline consistent with the domain growth observed in ferroelastic materials during second-order phase transitions [25].

In this sense, martensitic transformations in Ti–Nb alloys are first-order displacive transitions characterized by intrinsic energy barriers. The hysteresis results from the strain energy required to nucleate and propagate the martensite-austenite interface. During cooling, the $\beta \rightarrow \alpha''$ transformation requires subcooling to overcome the interfacial strain energy, while the reverse $\alpha'' \rightarrow \beta$ transformation during heating requires

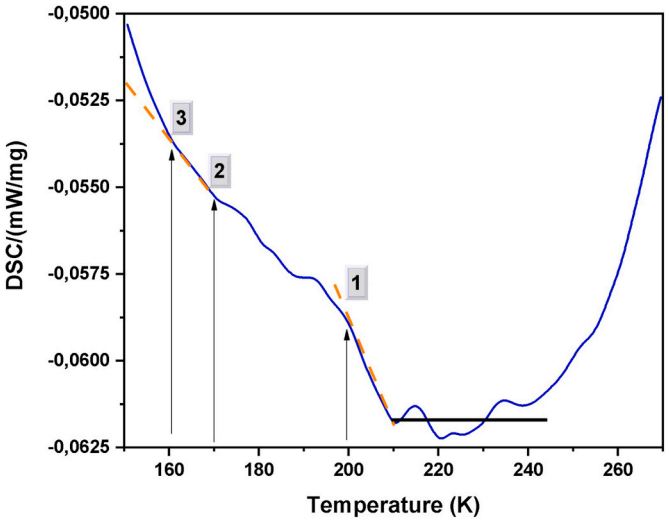

Fig. 5. DSC measurement realized in the TMZF sample.

superheating to overcome the same barrier [37]. Thus, cryogenic cooling traps metastable phases, such as ω-athermal and retained β-Ti phase, which modify the thermodynamic landscape and transformation kinetics. For example, it is reported [38] that in the Ti–23Nb-0.7Ta–2Zr (wt. %) alloy, planar ω-phase layers form at the α''/β interfaces during quenching. These ω-complexions reduce the interfacial energy and stabilize metastable configurations, effectively increasing the reverse transformation temperature (As) during heating. Here, the ω phase acts as a kinetic "lock" requiring additional thermal energy to dissolve before the $\alpha'' \rightarrow \beta$ transition can proceed.

Although ultrasonic velocity and attenuation have allowed us to obtain relevant information on the behavior of the sample under study at low temperatures, comparative DSC measurements were performed for comparison purposes, in cooling the sample at a rate of 10 K/min. Results are presented in Fig. 5. It is interesting to compare the DSC measurements in the same material in a cooling run, showing the anomalies 1, 2 and 3 at the same temperatures tagged in Fig. 3. Also, the irregular shape that it presents indicate a complex behaviour of the sample, like the observed in ultrasound spectrum in the corresponding temperature run. This is a clear indication that the anomalies identified in the ultrasonic spectrum correspond to certain mechanisms also detected through DSC measurements. The advantage of ultrasound is the ability to obtain information on the same sample for at least two parameters: attenuation and velocity. Furthermore, the system's temperature can be

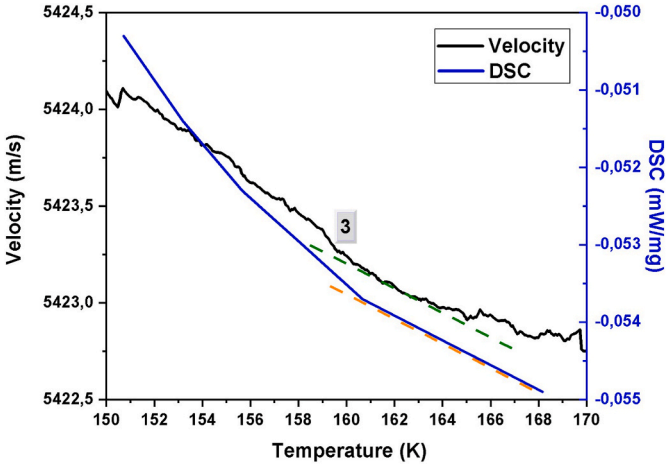

Fig. 6. Ultrasonic velocity in the cooling run and DSC curve of TMZF alloy amplified in the reduced temperature interval between 150 K and 170 K.

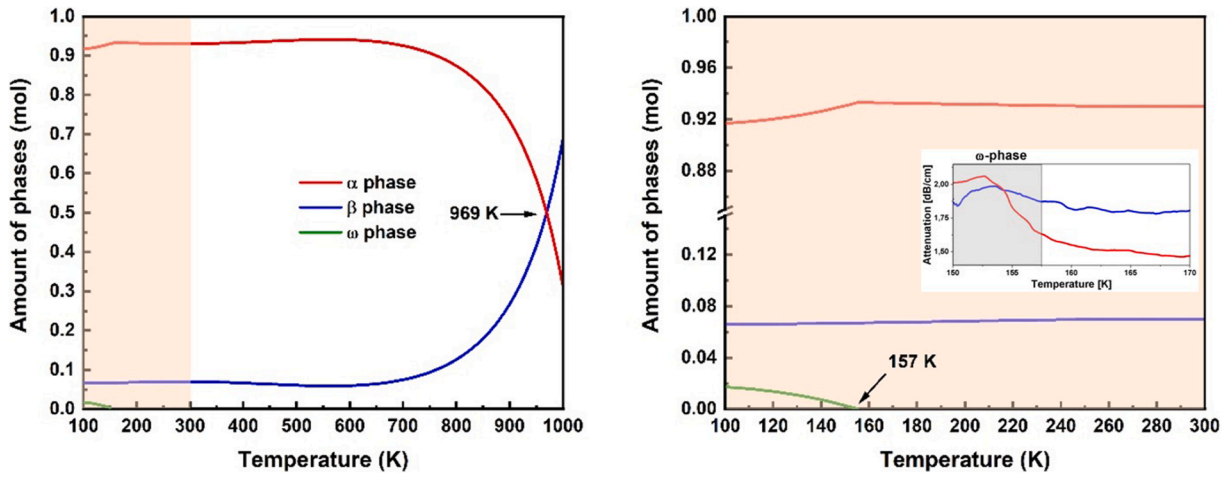

Fig. 7. Predicted phase proportion diagram by ThermoCalc®. In the right, zoomed view at the cryogenic temperatures, with attenuation also showing an anomaly compatible with the existence of the phase ω.

controlled with a very low rate of variation, ensuring the thermal uniformity of the sample throughout the measurement process. It is worth noting the complex structure of both measurements, ultrasonic and DSC. In general, both measurements show equivalent anomalies, some of which we identified and analyzed. Other minor anomalies may be attributed to complex mechanisms at the local scale, such as defects and/or wall interactions resulting from the TMZF sample composition and thermomechanical history. Guerra et al. [35] studied the effect of hot deformation in a beta metastable TMZF alloy with the same composition as the one analyzed by us. They detected this type of local mechanism at room temperature, which is typical of this kind of sample. We propose that this condition persists at temperatures below RT and is responsible for the observed minor anomalies.

The thermodynamic transition observed at temperatures above 160 K is characterized by a small amount of the α phase transforming into the ω phase. We expect only minor alterations in the cooling branch of both measurements (ultrasonic and DSC) due to the small amount of phase transformed as the temperature decreases. However, we can expect a more significant effect in the heating run. The velocity increases weakly in the cooling run and decreases more intensely in the heating run. As shown in Fig. 6, the ultrasonic velocity during the cooling run and the DSC curves are plotted in the temperature range of 150 K–170 K. An anomaly is observed in both curves at approximately 160 K, evidenced by the slope change in the curves.

3.3. *Theoretical phase prediction at cryogenic temperatures*

To better elucidate the anomalies of the ultrasonic measurements and the corresponding phase transitions, the phase composition at equilibrium of the TMZF alloy was further evaluated using the CALPHAD methodology. Fig. 7 shows that the α phase is stable at room temperature, transitioning to the β phase at high temperatures (~969 K), a typical polymorphic transition in Ti alloys. However, the image also depicts ω phase precipitation at a cryogenic temperature of 157 K, which was not previously detected in the literature using *in situ* characterization methods. The assumption of cryogenic ω phase precipitation is supported by some reports in the literature. Using thermodynamic approaches, Bonisch et al. [30] exploited the α, β, and ω phase proportions of Ti–Nb alloys as a temperature function. The results demonstrated the predominance of the ω phase at cryogenic temperatures, resulting from the β → ω phase transition. The same was reported by Hennig et al. [39], who pointed out the α → ω and β → ω phase transitions in metallic titanium as a function of pressure and temperature using *ab initio* methods. Finally, this finding is also supported by the Lai et al. [40] and Li et al. [41] reports, which explained the ω phase stability at low temperatures despite β in Ti–Nb and Ti–Nb–Ta–Zr alloys because of a spontaneous twinning in the $\{211\}_\beta < 111>_\beta$ boundary.

4. Conclusion

From the results reported in this study, it is possible to conclude.

- The as-received TMZF sample depicted a major β phase in the form of equiaxial grains and a minor martensitic α" phase with an aspect of thin acicular structure;
- Theoretical design methods also assured the presence of a metastable ω phase in the as-received sample;
- The ultrasonic characterization of the TMZF alloy at low temperatures showed several anomalies associated with equilibrium and non-equilibrium phenomena, as martensite phase transitions, changes in the morphology of martensite domain interfaces, complex mechanisms at the local scale, and a previously undetected cryogenic ω phase transition;
- The observed ultrasonic results reinforce the importance of this technique to study Ti-based alloys properties at low temperatures, where small changes in phase content and/or material morphology could be detected;
- To shed light on the mechanism responsible for the anomaly observed around 160K, the ThermoCalc® analysis obtained the corresponding phase diagram, which indicated the presence of the ω phase at cryogenic temperatures;
- The ultrasonic measurements allied to the theoretical methods proved to be an innovative way to detect phase transitions at cryogenic temperatures in Ti-based alloys, which can open new horizons for applications in extreme conditions, such as marine and aerospace environments.

Data availability

Data will be made available on request from authors.

Declaration of competing interest

The authors declare that they have no known competing financial interests or personal relationships that could have appeared to influence the work reported in this paper.

Acknowledgments

The authors thank the FAPESP (grant #2015/50.280-5 and BPE

grant #2024/05313-1), This study was financed in part by the Coordenação de Aperfeiçoamento de Pessoal de Nível Superior - Brasil (CAPES) - Finance Code 001., and CNPq (grant #308.204/2017-4 and #304.073/2019-9), research funding agencies from Brazil, and PEDECIBA (Program for the Development of Basic Sciences), research funding agency from Uruguay.

References

[1] Sarraf M, Rezvani Ghomi E, Alipour S, Ramakrishna S, Liana Sukiman N. A state-of-the-art review of the fabrication and characteristics of titanium and its alloys for biomedical applications. Biodes Manuf 2022;5:371–95. https://doi.org/10.1007/s42242-021-00170-3.

[2] Salvador CAF, Maia EL, Costa FH, Escobar JD, Oliveira JP. A compilation of experimental data on the mechanical properties and microstructural features of Ti-alloys. Sci Data 2022;9:1–6. https://doi.org/10.1038/s41597-022-01283-9.

[3] Kolli R, Devaraj A. A review of metastable beta titanium alloys. Metals 2018;8:506. https://doi.org/10.3390/met8070506.

[4] Elhadad AA, Romero-Resendiz L, Rossi MC, Rodríguez-Albelo LM, Lascano S, Afonso CRM, et al. Findings and perspectives of β-Ti alloys with biomedical applications: exploring beyond biomechanical and biofunctional behaviour. J Mater Res Technol 2024;33:3550–618. https://doi.org/10.1016/j.jmrt.2024.09.248.

[5] Chaves JM, Florêncio O, Silva PS, Marques PWB, Afonso CRM. Influence of phase transformations on dynamical elastic modulus and anelasticity of beta Ti–Nb–Fe alloys for biomedical applications. J Mech Behav Biomed Mater 2015;46:184–96. https://doi.org/10.1016/j.jmbbm.2015.02.030.

[6] Wang Q, Wu J, Tong L, Wang W, Yin R, Cao P. Phase transformation and kinetics in metastable β titanium alloy during isothermal treatment. Adv Eng Mater 2021;23:1–11. https://doi.org/10.1002/adem.202000709.

[7] Lopes ESN, Cremasco A, Afonso CRM, Caram R. Effects of double aging heat treatment on the microstructure, Vickers hardness and elastic modulus of Ti–Nb alloys. Mater Char 2011;62:673–80. https://doi.org/10.1016/j.matchar.2011.04.015.

[8] Tane M, Okuda Y, Todaka Y, Ogi H, Nagakubo A. Elastic properties of single-crystalline ω phase in titanium. Acta Mater 2013;61:7543–54. https://doi.org/10.1016/j.actamat.2013.08.036.

[9] Lai MJ, Li T, Yan FK, Li JS, Raabe D. Revisiting ω phase embrittlement in metastable β titanium alloys: role of elemental partitioning. Scr Mater 2021;193:38–42. https://doi.org/10.1016/j.scriptamat.2020.10.031.

[10] Li S, Choi M, Nam T. Role of fine nano-scaled isothermal omega phase on the mechanical and superelastic properties of a high Zr-containing Ti–Zr–Nb–Sn shape memory alloy. Mater Sci Eng, A 2020;782:139278. https://doi.org/10.1016/j.msea.2020.139278.

[11] Tito Patricio MA, Lustosa CJR, Chaves JAM, Marques PWB, Silva PS, Almeida A, et al. Relationship between microstructure, phase transformation, and mechanical behavior in Ti-40Ta alloys for biomedical applications. J Mater Res Technol 2021. https://doi.org/10.1016/j.jmrt.2021.06.038.

[12] Pilz S, Geissler D, Calin M, Eckert J, Zimmermann M, Freudenberger J, et al. Thermomechanical processing of In-containing β-type Ti-Nb alloys. J Mech Behav Biomed Mater 2018;79:283–91. https://doi.org/10.1016/j.jmbbm.2017.12.028.

[13] Zháňal P, Harcuba P, Šmilauerová J, Stráský J, Janeček M, Smola B, et al. Phase transformations in Ti-15Mo investigated by in situ electrical resistance. Acta Phys Pol, A 2015;128:779–82. https://doi.org/10.12693/APhysPolA.128.779.

[14] Gadeev DV, Illarionov AG. Determination of beta-transus temperature of two-phase titanium alloys using differential scanning calorimetry. Solid State Phenom 2018;284(SSP):259–64. https://dx.doi.org/10.4028/www.scientific.net/SSP.284.259.

[15] Behera M, Raju S, Mythili R, Saroja S. Study of kinetics of α ⇔ β phase transformation in Ti–4.4 mass% Ta–1.9 mass% Nb alloy using differential scanning calorimetry. J Therm Anal Calorim 2016;124:1217–28. https://doi.org/10.1007/s10973-016-5258-4.

[16] Nowick AS, Berry BS, Katz JL. Anelastic relaxation in crystalline solids. New York and London: Elsevier; 1972.

[17] Blanter MS, Golovin IS, Neuhäuser H, Sinning HR. Internal friction in metallic materials: a handbook, vol. 90; 2007. https://doi.org/10.1007/978-3-540-68758-0.

[18] Moreno-Gobbi A, Silva PS, Nespeque Correa DR, Milá AM, Muñoz Chaves JA, Grandini CR, et al. Experimental assessment of low-temperature martensite transformations in Ni-rich polycrystalline Ni–Ti alloys. J Mater Res Technol 2022;18:4990–5004. https://doi.org/10.1016/j.jmrt.2022.04.096.

[19] Ding C, Liu C, Zhang L, Wu D, Liu L. Design of low-cost and high-strength titanium alloys using pseudo-spinodal mechanism through diffusion couple technology and CALPHAD. Materials 2021;14:2910. https://doi.org/10.3390/ma14112910.

[20] Liang Z, Miao J, Brown T, Sachdev AK, Williams JC, Luo AA. A low-cost and high-strength Ti-Al-Fe-based cast titanium alloy for structural applications. Scr Mater 2018;157:124–8. https://doi.org/10.1016/j.scriptamat.2018.08.005.

[21] Wu Y, Liaw PK, Li R, Zhang W, Geng G, Yan X, et al. Relationship between the unique microstructures and behaviors of high-entropy alloys. Int J Miner Metall Mater 2024;31:1350–63. https://doi.org/10.1007/s12613-023-2777-4.

[22] Santos RFM, Ricci VP, Afonso CRM. Influence of swaging on microstructure, elastic modulus and Vickers microhardness of β Ti-40Nb alloy for implants. J Mater Eng Perform 2021;30:3363–9. https://doi.org/10.1007/s11665-021-05706-3.

[23] Santos RFM, Ricci VP, Afonso CRM. Continuous cooling transformation (CCT) diagrams of β Ti-40Nb and TMZF alloys and influence of cooling rate on microstructure and elastic modulus. Thermochim Acta 2022;717:179341. https://doi.org/10.1016/j.tca.2022.179341.

[24] de Mello MG, Salvador CAF, Costa FH, Campo KN, Afonso CRM, Cremasco A, et al. Phase evolution and spinodal decomposition in Ti-13Mo-2Fe during aging. Metall Mater Trans 2024;55:4742–6. https://doi.org/10.1007/s11661-024-07601-7.

[25] Lüthi B. Physical acoustics in the solid state, vol. 148. Berlin, Heidelberg: Springer Berlin Heidelberg; 2005. https://doi.org/10.1007/978-3-540-72194-9.

[26] Moreno-Gobbi A, Moreno D, Zamir G. Ultrasonic study of structural instabilities in nickel induced by magnetic fields. Mater Res 2008;11:31–5. https://doi.org/10.1590/S1516-14392008000100006.

[27] Thoemmes A, Bataev IA, Lazurenko DV, Ruktuev AA, Ivanov IV, Afonso CRM, Stark A, Jorge AM. Microstructure and Lattice Parameters of Suction-Cast Ti-Nb Alloys in a Wide Range of Nb Concentrations. Mater Sci Eng A 2021;817:141378. https://doi.org/10.1016/j.msea.2021.141378.

[28] Santos RFM, Rossi MC, Vidilli AL, Amigó VB, Afonso CRM. Assessment of β stabilizers additions on microstructure and properties of as-cast β Ti-Nb based alloys. J Mater Res Technol 2022;22:3511–24. https://doi.org/10.1016/j.jmrt.2022.12.144.

[29] Murray N, Jablokov V, Freese H. Mechanical and physical properties of Titanium-12Molybdenum-6Zirconium-2Iron beta titanium alloy. J ASTM Int (JAI) 2005;2:1–13. https://doi.org/10.1520/JAI12774.

[30] Wong K-K, Hsu H-C, Wu S-C, Ho W-F. A review: design from beta titanium alloys to medium-entropy alloys for biomedical applications. Materials 2023;16:7046. https://doi.org/10.3390/ma16217046.

[31] Attallah MM, Zabeen S, Cernik RJ, Preuss M. Comparative determination of the α/β phase fraction in α+β-titanium alloys using X-ray diffraction and electron microscopy. Mater Char 2009;60:1248–56. https://doi.org/10.1016/j.matchar.2009.05.006.

[32] Cotton JD, Briggs RD, Boyer RR, Tamirisakandala S, Russo P, Shchetnikov N, et al. State of the art in beta titanium alloys for airframe applications. J Occup Med 2015;67:1281–303. https://doi.org/10.1007/s11837-015-1442-4.

[33] Marković G, Manojlović V, Ružić J, Sokić M. Predicting low-modulus biocompatible titanium alloys using machine learning. Materials 2023;16:6355. https://doi.org/10.3390/ma16196355.

[34] ASTM F1813-01. Standard specification for titanium-12Molybdenum-6zirconium-2iron alloy for surgical implant applications. 2017.

[35] Guerra AP de B, Jorge AM, Roche V, Bolfarini C. Hot deformation behavior of a beta metastable TMZF alloy: microstructural and constitutive phenomenological analysis. Metals 2021;11:1769. https://doi.org/10.3390/met11111769.

[36] Nag S, Banerjee R, Stechschulte J, Fraser HL. Comparison of microstructural evolution in Ti-Mo-Zr-Fe and Ti-15Mo biocompatible alloys. J Mater Sci Mater Med 2005;16:679–85. https://doi.org/10.1007/s10856-005-2540-6.

[37] Chang H, Gautier EA, Zhou L. Phase transformation kinetics in metastable titanium alloys. Chin Sci Bull 2014;59:1773–7. https://doi.org/10.1007/s11434-014-0210-0.

[38] Zhang J, Tasan CC, Lai MJ, Dippel A-C, Raabe D. Complexion-mediated martensitic phase transformation in Titanium. Nat Commun 2017;8:14210. https://doi.org/10.1038/ncomms14210.

[39] Hennig RG, Trinkle DR, Bouchet J, Srinivasan SG, Albers RC, Wilkins JW. Impurities block the α to ω martensitic transformation in titanium. Nat Mater 2005;4:129–33. https://doi.org/10.1038/nmat1292.

[40] Lai MJ, Tasan CC, Zhang J, Grabowski B, Huang LF, Raabe D. Origin of shear induced β to ω transition in Ti–Nb-based alloys. Acta Mater 2015;92:55–63. https://doi.org/10.1016/j.actamat.2015.03.040.

[41] Li Y, Liao Z, Zhang W, Wu Z, Zhou C. Strength-ductility synergy in a metastable β titanium alloy by stress induced interfacial twin boundary ω phase at cryogenic temperatures. Materials 2020;13:4732. https://doi.org/10.3390/ma13214732.